

Multiple representation of the elastic field of dislocation ensembles

Zhiqiang Wang and Nasr Ghoniem

Department of Mechanical and Aerospace Engineering, University of California, Los Angeles, Los Angeles, California 90095, USA

Richard LeSar

Theoretical Division, T-12, MS B268, Los Alamos National Laboratory, Los Alamos, New Mexico 87545, USA

(Received 23 December 2003; published 7 May 2004)

A multipole expansion method is developed to determine the elastic field of dislocation loop ensembles of arbitrary geometric complexity. The method results in reduction of the severe computational requirements in large-scale dislocation dynamics (DD) computer simulations without an artificial cutoff on the interaction range. Order of N , $O(N)$, algorithms for DD simulations is immediately accessible on the basis of the developed procedure. Examples of dislocation interaction with large dislocation arrays representing a tilt boundary and a dislocation wall show that the method results in speeding up the calculation of Peach-Koehler interaction forces by a factor of 100, with an error of less than 0.4%. The multipole expansion reveals a physical connection to Kröner's continuum theory of dislocations, with the zeroth order moment being Nye's dislocation density tensor. Higher-order tensors in the expansion correspond to moments of a basic tensor comprised of the tangent and Burgers vectors, and can be used to characterize the spatial distribution of dislocation loop ensembles.

DOI: 10.1103/PhysRevB.69.174102

PACS number(s): 61.72.Lk, 02.60.Cb

I. INTRODUCTION

The development of a physically based theory of plasticity has been one of the most challenging endeavors attempted in recent years. Despite the recognition of the inadequacy of continuum mechanics to resolve important features of plastic deformation, attempts to include the physics of plastic deformation through constitutive relations are far from satisfactory. This is particularly evident for the resolution of critical phenomena, such as plastic instabilities, work hardening, fatigue crack initiation, persistent slip band formation, etc.

An alternative method for providing access to the physics of plastic deformation at the mesoscale is the direct numerical simulation of discrete dislocation microstructure evolution, which is commonly known as the dislocation dynamics (DD) method.¹⁻⁷

Although DD has been successfully applied to a wide range of physical problems, especially for problems involving length scales in the 10^{-9} – 10^{-6} range,^{8,9} the extension of the approach to larger length scales (e.g., for application in polycrystalline material deformation) is still a daunting task. The main impediment in this direction is the lack of methods for systematic and rigorous “coarse graining” of discrete dislocation processes. Notable recent developments in this area have been advanced by Lesar and Rickman.¹⁰

The main objective of the present work is to develop a coarse-graining approach for evaluation of the elastic field of large dislocation loop ensembles of arbitrary geometric complexity. The method is an extension of the Lesar-Rickman multipole expansion of the elastic energy of dislocation ensembles.¹⁰ The broad coarse-graining objective of the present work is associated with a number of motivating reasons for this development, as given below.

- (1) To access the physics of plasticity through direct

large-scale computer simulations of dislocation microstructure evolution. This is enabled by a substantial reduction of the speed of computation.

- (2) To remove the cutoff distance limitation in dislocation-dislocation interactions, and hence facilitate our understanding of microstructure evolution sensitivity to such computational limitation.

- (3) To allow efficient determination of the “effective” influence of dislocation arrays (e.g., in some representation of grain boundaries), or complex dislocation blocks (e.g., in dislocation walls and tangles) on the interaction with approaching dislocations.

- (4) To enable embedding into well established, $O(N)$, computational procedures for particle systems of long-range interactive force fields.¹¹

- (5) To shed more light on the connection between discrete dislocation dynamics, the Kröner-Kosevich continuum theory of dislocations,¹² and moments of a basic local tensor that characterize the spatial distribution of dislocations.

We present the multipole expansion method (MEM) formulation in Sec. II. In $O(N)$ methods for calculation of the effective fields in particle systems with long-range interaction force fields, moments evaluated for smaller volumes are usually transferred or combined with moments defined in other volumes. This issue will be explained in Sec. III. Results for the far-field expansion of the stress field and interaction forces are given in Sec. IV, while applications of the method to dislocation arrays in special boundaries or dislocation walls are presented in Sec. V. Finally conclusions of this work are presented in Sec. VI.

II. FORMULATION OF THE MULTIPOLE REPRESENTATION

The stress field at any point from a single closed dislocation loop can be written as¹³

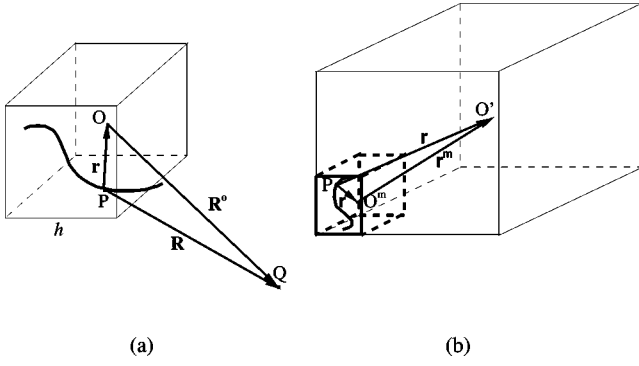


FIG. 1. Illustration of the geometries of (a) a single volume with center O containing dislocations, (b) a single volume (center O') containing many small volumes with centers O^m .

$$\sigma_{ij} = \frac{\mu b_n}{8\pi} \oint \left[R_{,mpp} (\epsilon_{jmn} dl_i + \epsilon_{imn} dl_j) + \frac{2}{1-\nu} \epsilon_{kmn} (R_{,ijm} - \delta_{ij} R_{,ppm}) dl_k \right], \quad (1)$$

where $\mathbf{R} = \mathbf{Q} - \mathbf{P}$ is the vector connecting field point Q and source point P at dislocations [Fig. 1(a)]. The stress field per unit volume of an ensemble of dislocation loops in a volume Ω , some of them may not be closed within Ω , is given by

$$\sigma_{ij} = \frac{\mu}{8\pi\Omega} \left\{ \sum_{\xi=1}^{N_L^{closed}} \oint_{\xi} \left[R_{,mpp} (\epsilon_{jmn} dl_i + \epsilon_{imn} dl_j) + \frac{2}{1-\nu} \epsilon_{kmn} (R_{,ijm} - \delta_{ij} R_{,ppm}) dl_k \right] + \sum_{\xi=N_L^{closed}+1}^{N_L} \int_{\xi} \left[R_{,mpp} (\epsilon_{jmn} dl_i + \epsilon_{imn} dl_j) + \frac{2}{1-\nu} \epsilon_{kmn} (R_{,ijm} - \delta_{ij} R_{,ppm}) dl_k \right] \right\}, \quad (2)$$

where N_L^{closed} is the number of closed dislocation loops within the volume Ω , N_L^{open} is the number of open dislocation loops, which intersect the surfaces of the volume Ω , $N_L = N_L^{closed} + N_L^{open}$ is the total number of dislocation loops in the volume Ω .

Suppose that the distance between point P on a dislocation and a field point Q is relatively larger than the size h of a certain volume that contains the dislocation loop, as shown in Fig. 1. Point O is the center of the volume. Let us write the Taylor-series expansion of the derivatives of vector \mathbf{R} at point O as follows:

$$R_{,ijm} = R_{,ijm}^o + R_{,ijmk}^o r_k + \frac{1}{2!} R_{,ijmkl}^o r_k r_l + \frac{1}{3!} R_{,ijmklm}^o r_k r_l r_n + \dots, \quad (3)$$

where $\mathbf{r} = \mathbf{O} - \mathbf{P}$ and $\mathbf{R}^o = \mathbf{Q} - \mathbf{O}$.

Substituting these expansions in Eq. (2), and recognizing that $R_{,mpp}^o$, $R_{,ijm}^o$, $R_{,ppm}^o$ and their higher-order derivatives depend only on \mathbf{R}^o , we find

$$\sigma_{ij} = \frac{\mu}{8\pi} \left\{ \left[R_{,mpp}^o (\epsilon_{jmn} \alpha_{ni} + \epsilon_{imn} \alpha_{nj}) + R_{,mppq}^o (\epsilon_{jmn} \beta_{niq} + \epsilon_{imn} \beta_{njq}) + \frac{1}{2!} R_{,mppqs}^o (\epsilon_{jmn} \gamma_{niqs} + \epsilon_{imn} \gamma_{njqs}) + \frac{1}{3!} R_{,mppqst}^o (\epsilon_{jmn} \psi_{niqst} + \epsilon_{imn} \psi_{njqst}) + \dots \right] + \frac{2}{1-\nu} \epsilon_{kmn} \left[R_{,ijm}^o \alpha_{nk} + R_{,ijmq}^o \beta_{nkq} + \frac{1}{2!} R_{,ijmqs}^o \gamma_{nkqs} + \frac{1}{3!} R_{,ijmqst}^o \psi_{nkqst} + \dots \right] - \frac{2}{1-\nu} \delta_{ij} \epsilon_{kmn} \left[R_{,ppm}^o \alpha_{nk} + R_{,ppmq}^o \beta_{nkq} + \frac{1}{2!} R_{,ppmqs}^o \gamma_{nkqs} + \frac{1}{3!} R_{,ppmqst}^o \psi_{nkqst} + \dots \right] \right\}, \quad (4)$$

where we define the dislocation moments of zeroth order within the volume Ω as

$$\alpha_{ij} = \frac{1}{\Omega} \sum_{\xi=1}^{N_L^{closed}} \oint_{\xi} E_{ij}^{\xi} dl + \frac{1}{\Omega} \sum_{\xi=N_L^{closed}+1}^{N_L} \int_{\xi} E_{ij}^{\xi} dl = \frac{1}{\Omega} \sum_{\xi=N_L^{closed}+1}^{N_L} \int_{\xi} E_{ij}^{\xi} dl, \quad (5)$$

where $dl = |dl|$ is an infinitesimal line length along the unit tangent \mathbf{t} . The Eshelby rational tensor E_{ij} , defined as $E_{ij}^{\xi} = b_i^{\xi} t_j^{\xi}(\mathbf{P})$, is a local tensor because it is defined at point \mathbf{P} on a loop ξ , where t_j^{ξ} is the tangent vector at position \mathbf{P} and \mathbf{b}^{ξ} is the Burgers vector of the loop. It is clear that the only contribution to the tensor α_{ij} is from open loops (i.e., the second term), since the contribution of closed-loops is identically zero by virtue of the closed-loop property. Equation (5) gives Nye's dislocation density tensor α_{ij} .^{14,15} This tensor is directly related to the lattice curvature tensor $\boldsymbol{\kappa}$ by¹²

$$\boldsymbol{\kappa} = \frac{1}{2} \text{Tr}(\boldsymbol{\alpha}) \mathbf{I} - \boldsymbol{\alpha}, \quad (6)$$

where \mathbf{I} is the second-order unit tensor. Higher-order tensors $\boldsymbol{\beta}, \boldsymbol{\gamma}, \boldsymbol{\psi}, \dots$ correspond to higher-order moments of the Eshelby rational tensor, and are defined as

$$\beta_{ijk} = \frac{1}{\Omega} \sum_{\xi=1}^{N_L} \int_{\xi} r_k E_{ij} dl, \quad \gamma_{ijkl} = \frac{1}{\Omega} \sum_{\xi=1}^{N_L} \int_{\xi} r_k r_l E_{ij} dl,$$

$$\begin{aligned}\psi_{ijklq} &= \frac{1}{\Omega} \sum_{\xi=1}^{N_L} \int_{\xi} r_k r_l r_q E_{ij} dl, \\ \zeta_{ijklq \dots p} &= \frac{1}{\Omega} \sum_{\xi=1}^{N_L} \int_{\xi} r_k r_l r_q \dots r_p E_{ij} dl.\end{aligned}\quad (7)$$

We can write the stress field resulting from a dislocation ensemble within the volume Ω as

$$\begin{aligned}\sigma_{ij} &= \frac{\mu\Omega}{8\pi} \sum_{t=0}^{\infty} \frac{1}{t!} \left[R_{,m p p a_1 \dots a_t}^o \langle \epsilon_{jmn} \langle \zeta_{nia_1 \dots a_t} \rangle \right. \\ &\quad + \epsilon_{imn} \langle \zeta_{nja_1 \dots a_t} \rangle + \frac{2}{1-\nu} \epsilon_{kmn} R_{,ijma_1 \dots a_t}^o \langle \zeta_{nka_1 \dots a_t} \rangle \\ &\quad \left. - \frac{2}{1-\nu} \delta_{ij} \epsilon_{kmn} R_{,ppma_1 \dots a_t}^o \langle \zeta_{nka_1 \dots a_t} \rangle \right],\end{aligned}\quad (8)$$

where $\langle \zeta_{ijk \dots} \rangle$ represent the moments defined above different orders, as α_{ij} , β_{ijk} , γ_{ijkl} , etc. These moments depend only on the selected center point O and the distribution of the dislocation microstructure within the volume. They can be evaluated for each volume independently. After the moments are determined, the stress field and interaction forces on other dislocations that are sufficiently well separated from the volume Ω are easily obtained.

III. RULES FOR COMBINATION OF MOMENTS

For a fixed field point, if the distance of a volume to this point is larger than its characteristic size, we can utilize moments obtained from smaller subvolumes to generate moments for the total volume. This procedure is similar to the ‘‘parallel axis theorem’’ for shifting moments of inertia for mass distributions in mechanics. Suppose that this large volume is composed of several subvolumes and we have multipole expansions for each subvolume, we develop here a procedure to obtain multipole expansion for the large volume from those for the subvolumes instead of doing the calculations again for each dislocation loop. This idea is very suitable for hierarchical tree algorithms, such as the Greengard-Rokhlin method.¹⁶ We will describe formulations for combination of multipole expansions in this section.

Assume that a large material volume Ω centered at \mathbf{O}' contains M small subvolumes centered at O^m , with their volumes as Ω^m , where m is an index [Fig. 1 (b)]. Here, \mathbf{r}^m is the vector connecting O^m and O' . The new vector connecting the center O' and a point on a dislocation is $\mathbf{r}' = \mathbf{r} + \mathbf{r}^m$, where $\mathbf{r}^m = \mathbf{O}' - \mathbf{O}^m$. With the dislocation moments for the m th small material volume as α_{ij}^m , β_{ijk}^m , . . . , we can write the moments of dislocations in the m th subvolume in the large volume as follows:

$$\alpha_{ij}^{m'} = \frac{1}{\Omega} \sum_{\xi \in N_L^{closed^m} + 1}^{N_L^m} \int_{\xi} E_{ij}^{\xi} dl = f^m \alpha_{ij}^m,$$

$$\begin{aligned}\beta_{ijk}^{m'} &= \frac{1}{\Omega} \sum_{\xi=1}^{N_L^m} \int_{\xi} r'_k E_{ij}^{\xi} dl = \frac{1}{\Omega} \sum_{\xi=1}^{N_L^m} \int_{\xi} (r_k + r_k^m) E_{ij}^{\xi} dl \\ &= \frac{1}{\Omega} \sum_{\xi=1}^{N_L^m} \int_{\xi} r_k E_{ij}^{\xi} dl + \frac{1}{\Omega} \sum_{\xi=1}^{N_L^m} \int_{\xi} r_k^m E_{ij}^{\xi} dl \\ &= f^m (\beta_{ijk}^m + r_k^m \alpha_{ij}^m), \\ \gamma_{ijkl}^{m'} &= \frac{1}{\Omega} \sum_{\xi=1}^{N_L^m} \int_{\xi} r'_k r'_l E_{ij}^{\xi} dl \\ &= f^m (\gamma_{ijkl}^m + r_k^m \beta_{ijl}^m + r_l^m \beta_{ijk}^m + r_k^m r_l^m \alpha_{ij}^m), \\ &\quad \dots,\end{aligned}\quad (9)$$

where $f^m = \Omega^m / \Omega$, N_L^m and $N_L^{closed^m}$ are volume fraction, the number of total dislocation loops, and the number of closed loops in the m th volume, respectively.

Then, the total moments of dislocation loop distributions within the large volume are given by

$$\begin{aligned}\alpha_{ij} &= \sum_{m=1}^M \alpha_{ij}^{m'} = \sum_{m=1}^M f^m \alpha_{ij}^m, \\ \beta_{ijk} &= \sum_{m=1}^M \beta_{ijk}^{m'} = \sum_{m=1}^M f^m (\beta_{ijk}^m + r_k^m \alpha_{ij}^m), \\ \gamma_{ijkl} &= \sum_{m=1}^M \gamma_{ijkl}^{m'} = \sum_{m=1}^M f^m (\gamma_{ijkl}^m + r_k^m \beta_{ijl}^m + r_l^m \beta_{ijk}^m + r_k^m r_l^m \alpha_{ij}^m), \\ &\quad \dots.\end{aligned}\quad (10)$$

Equation (10) can be written in a compact form as

$$\begin{aligned}\zeta_{ija_1 \dots a_n} &= \sum_{m=1}^M f^m \left\{ \sum_{p=0}^n \left[\sum_{q=1}^{C_n^p} [(r_{t_1}^m r_{t_2}^m \dots r_{t_p}^m) \right. \right. \\ &\quad \left. \left. \times \langle \zeta_{ijt_{p+1} \dots t_n}^m \rangle \right] \right\},\end{aligned}\quad (11)$$

where $n=0,1,2, \dots$ is the order of the moment. Here, $\sum_{q=1}^{C_n^p}$ means that r^m 's subindex group of t_1, \dots, t_p are selected from the n index group of a_n in a permutational manner, and group of indices t_{p+1}, \dots, t_n are the corresponding $n-p$ indices of a_n after the selection.

IV. NUMERICAL RESULTS

Based on the equations developed in the previous sections, we numerically implement here the multipole expansion for the stress field of a dislocation ensemble, expressed by Eq. (8). We consider here the results of the full calculation based on Eq. (2) as reference, and calculate relative errors from the MEM as $|\sigma_{MEM} - \sigma_{ref}| / \sigma_{ref}$. Tests are performed on a volume with $h=10 \mu\text{m}$ for different expansion orders

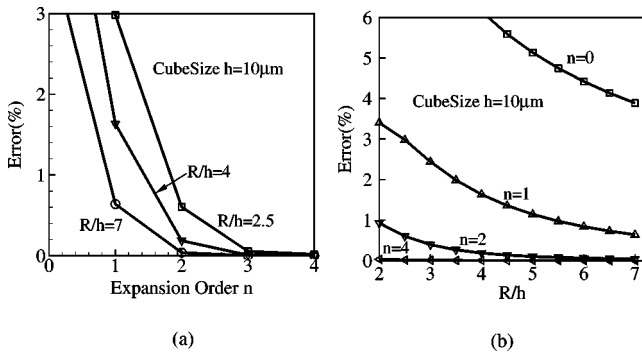


FIG. 2. Relative error of the MEM vs (a) the expansion order n , (b) the R/h value for a simulation volume with an edge length of $10 \mu\text{m}$.

and different values of R/h . Dislocations are generated randomly inside the volume and with a density of $5 \times 10^8 \text{ cm}^{-3}$. Numerical results are shown in Fig. 2. From these results, it is clear that the approximate moment solutions converge fast. For different values of R/h , the second-order expansion gives a relative error less than 1%, while the fourth-order expansion gives a relative error less than 0.05%.

V. APPLICATIONS TO DISLOCATION BOUNDARIES AND WALLS

A. Dislocation interaction with a tilt boundary

An important consequence of heavy plastic deformation is the rearrangement of dislocations into well-separated tangles or periodic arrays. Dislocation tangles evolve into walls that can act as sources of new dislocations, or stop approaching glide dislocations from neighboring volumes. On the other hand, some grain boundaries can be represented by dislocation arrays. The elastic field generated by grain boundaries in compatibility can thus be determined from the dislocation array representing its structure. Such dislocation microstructures have profound effect on the deformation characteristics of materials, and more often, some effective properties are needed. In this section, we investigate the feasibility of effective elastic representation of periodic dislocation arrays and dislocation walls utilizing the MEM derived earlier. We will first analyze the effective influence of a tilt boundary on the deformation of a dislocation emitted from a nearby Frank-Read (F-R) source. We will then investigate the nature of the Peach-Koehler force on dislocations approaching a dense entanglement of dislocations within a dislocation wall. The following examples are for single crystal Cu, with the following parameters: shear modulus $\mu = 50 \text{ GPa}$, lattice constant $a = 3.615 \times 10^{-10} \text{ m}$, Poisson's ratio $\nu = 0.31$.

Figure 3 shows the geometry of a 1° tilt boundary containing 35 dislocations with $\frac{1}{2}[\bar{1}01]$ Burgers vector. A F-R source is located $1 \mu\text{m}$ away from the tilt boundary. The source, which lies on the $[111]$ glide plane, emits dislocations with $[\bar{1}2\bar{1}]$ tangent vector and $\frac{1}{2}[\bar{1}01]$ Burgers vector as well. The initial length of the F-R source dislocation between pinned ends is $700a$. A constant uniaxial stress of 25 MPa is applied in the $[100]$ direction.

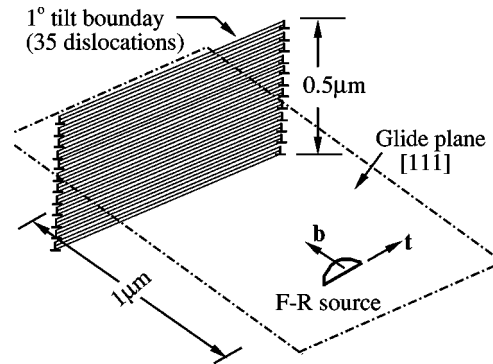


FIG. 3. Illustration of a tilt boundary. A single dislocation from an F-R source lies on the $[111]$ glide plane with Burgers vector $\frac{1}{2}[\bar{1}01]$ interacts with the tilt boundary.

Dislocation motion under the influence of the externally applied stress and the internal stress generated by the tilt boundary is determined by using the method of parametric dislocation dynamics.^{3,13} Interaction forces between the tilt boundary and the F-R source dislocation are calculated by two methods: (1) the fast sum method,² which adds up the contributions of every dislocation segment within the boundary; (2) the current MEM up to second-order quadrupole term. Dislocation configurations at different time steps are shown in Fig. 4(a). The relative error in the MEM in the position of the dislocation (at its closest point to the tilt boundary) is shown in Fig. 4(b). The results of the simulation show that the MEM is highly accurate (error on the order of 0.4%), and that the overall dislocation configuration is indistinguishable when evaluated by the two methods. However, the MEM is found to be 22 times faster than the full field calculation.

B. Dislocation interaction with a dense dislocation wall

The physical role of dislocation walls in material deformation is recognized to be significant because they control the free path of mobile dislocations within subgrains.¹⁷ Dislocation walls generally contain high dislocation densities. Therefore, explicit large-scale simulation of the interaction between these walls and approaching dislocations can present computational difficulties. If the nature of decay of

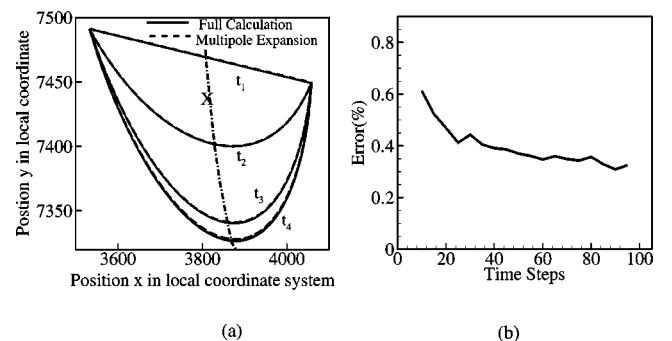


FIG. 4. (a) Dislocation configurations at different simulation time steps: $t_1=0 \text{ ns}$, $t_2=0.31 \text{ ns}$, $t_3=0.62 \text{ ns}$, $t_4=1.23 \text{ ns}$; (b) relative error of the dislocation position along the line X in (a).

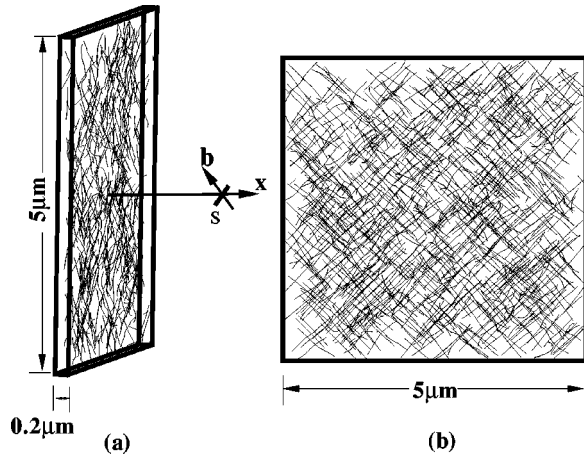


FIG. 5. Dislocation wall structure with dislocation density 5×10^{10} cm/cm³. A small dislocation segment S with Burgers vector $\frac{1}{2}[10\bar{1}]$ lies along x .

the elastic field away from the wall is determined, this would be helpful in studies of dislocation interaction with such walls without the excessive details.

A special algorithm was designed to implement the MEM in dense dislocation walls. The wall was divided into many small volumes, and a hierarchical tree structure was constructed on the basis of these small volumes. Each level of the hierarchical tree contains one or several nodes that correspond to specific volumes of the wall. Larger volumes correspond to higher levels of the tree. For each volume, we determine the properties: center, size, dislocation distribution, and various moments. Dislocation moments for the lowest level volumes are first calculated. Then, by using Eq. (11), dislocation moments for upper tree levels can be easily determined.

The procedure for calculations of the Peach-Koehler (P-K) force on an approaching dislocation at point P is as follows.

- (1) The distance between the volume center and the point P is first evaluated. If the distance is larger than the volume's size, MEM is used.
- (2) If the distance is smaller than the volume size and the volume does not have sub-volumes, the P-K force is determined by full calculation.
- (3) If the distance is smaller than the volume's size and the volume has subvolumes, the algorithm checks on the distance between P and the center of each subvolume, and the above procedures are repeated.

Figure 5 shows a dislocation wall structure with a density of 5×10^{10} cm/cm³. The wall dimensions are $5 \times 5 \times 0.2 \mu\text{m}^3$. The P-K force on a small dislocation segment, located at various positions along the center line X , with Burgers vector $\frac{1}{2}[10\bar{1}]$ was evaluated by both MEM and full calculations. The results of the P-K force and the relative errors are plotted in Fig. 6.

While the relative error using MEM of order 2 is very small [see Figure 6(b)], a great advantage in computational speed is gained. The results show that the CPU time (on a Pentium-4 CPU, 2.26 GHz) increases almost linearly from

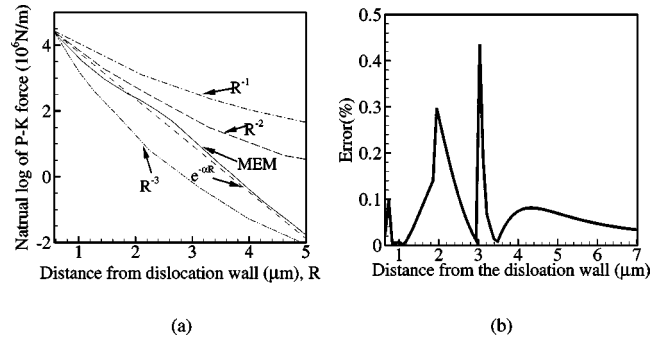


FIG. 6. (a) P-K forces on a small dislocation segment at different positions along direction x , (b) relative error of the P-K force from MEM with respect to that from full calculation.

416 sec to 3712 sec for the full calculation, when the number of dislocations in the wall increases from 250 to 2200. However, the CPU time does not change much for the MEM (varying from 39 sec to 40 sec) for the same increase in the number of dislocations. For the case of 2200 dislocations within the wall, a speedup factor of almost 100 is achieved for the MEM. Recognizing that the CPU time for the MEM is almost constant and mostly dependent on the hierarchical tree structure, it is concluded that the method is very suitable for large-scale simulations, which involve high dislocation densities.

It is of interest to determine the decay nature of the elastic field emanating from dislocation walls. Figure 6(a) shows a comparison between various forms of the spatial decay of the P-K force as a function of the distance R away from the wall, normalized to the force at $R_0 = 0.59 \mu\text{m}$. It is seen that the force decays faster than R^{-2} , and it can be simply represented by an exponential function of the form

$$F(R) = F(R_0)e^{-\alpha(R-R_0)}, \quad (12)$$

where $\alpha = 1.36 \mu\text{m}^{-1}$. Such simple exponential representation is a result of the self-shielding of the dislocations within the wall.

VI. CONCLUSIONS

The MEM presented here shows a number of features that facilitates investigation into the physical and computational aspects of large dislocation ensembles in materials undergoing plastic deformation. The following conclusions are drawn from the present work.

(1) By re-expressing the elastic field of dislocation ensembles as a series solution of moments, the relative contributions of open loops, dipoles, quadrupoles, etc., are easily separated out.

(2) The method results in significant computational advantages as compared to calculations performed in most dislocation dynamics simulation method. First, vast computational speedup is achieved, especially in simulations of dense dislocation interactions. Second, the method offers a simple algebraic procedure for transfer of moments from one volume to another, in a manner similar to the parallel axis theo-

rem for moments of inertia in the mechanics of distributed masses. This property is well suited to algorithms based on hierarchical tree methods that are now efficiently used in $O(N)$ calculations.

(3) The zeroth order term in the MEM expansion is the Nye's dislocation density tensor, which is a direct measure of lattice curvature, and is affected only by open dislocation loops within the ensemble. Diagonal components of this tensor describe screw dislocations, while off-diagonal components represent edge dislocations. On the other hand, higher-order moments of the Eshelby tensor are associated with definite length-scale measures that may be useful in connections between discrete dislocation simulations and the continuum theory of dislocations.

(4) The analysis of dense dislocation walls indicates that the Peach-Koehler force has an exponential decay character as a result of mutual shielding effects of multipole dislocations within random ensemble constituting the walls.

ACKNOWLEDGMENTS

The work at UCLA was performed under Contract No. 54280-001-03 2F with Los Alamos National Laboratory. The work of R. LeSar was performed under the auspices of the United States Department of Energy (US DOE) under Contract No. W-7405-ENG-36 and was supported in part by the Division of Materials Science of the Office of Basic Energy Sciences of the Office of Science of the US DOE.

APPENDIX A: \mathbf{R} AND ITS DERIVATIVES

\mathbf{R} is the vector connecting field point Q and another point P on the dislocation or O , center of the volume (see Fig. 1). \mathbf{R} and its derivatives are used in expressions of displacements, strains, stresses, and energies of dislocations.¹³ Here, we define a way to express \mathbf{R} and its derivatives in compact tensor forms.

Define

$$\mathbf{R} = \{x_{ij}\} \quad \text{and} \quad \mathbf{g} = \left\{ \frac{x_i}{R} \right\}, \quad (\text{A1})$$

where $R = |\mathbf{R}|$. Thus,

$$R_{,i} = \frac{x_i}{R} = g_i, \quad (\text{A2})$$

$$R_{,ij} = \frac{\delta_{ij}}{R} - \frac{x_i x_j}{R^3} = -\frac{1}{R} (-\delta_{ij} + g_i g_j), \quad (\text{A3})$$

$$\begin{aligned} R_{,ijk} &= -\frac{\delta_{jk} x_i + \delta_{ik} x_j + \delta_{ij} x_k}{R^3} + \frac{3x_i x_j x_k}{R^5} \\ &= \frac{1}{R^2} [-(\delta_{jk} g_i + \delta_{ik} g_j + \delta_{ij} g_k) + 3g_i g_j g_k], \end{aligned} \quad (\text{A4})$$

$$\begin{aligned} R_{,ijkl} &= -\frac{\delta_{ij} \delta_{kl} + \delta_{ik} \delta_{jl} + \delta_{il} \delta_{jk}}{R^3} + \frac{3(\delta_{jk} x_i x_l + \delta_{ik} x_j x_l + \delta_{ij} x_k x_l + \delta_{kl} x_i x_j + \delta_{jl} x_i x_k + \delta_{il} x_j x_k)}{R^5} - \frac{3 \times 5 x_i x_j x_k x_l}{R^7} \\ &= \frac{1}{R^3} [(\delta_{ij} \delta_{kl} + \dots) - 3(\delta_{jk} g_i g_l + \dots) + 3 \times 5 g_i g_j g_k g_l], \end{aligned} \quad (\text{A5})$$

$$\dots \quad (\text{A6})$$

Based on the above derivations and after careful analysis, we can write these derivatives as

$$\begin{aligned} R_{,a_1 a_2 \dots a_n} &= \left(\frac{-1}{R} \right)^{n-1} \sum_{m=0}^{\lfloor n/2 \rfloor} \left\{ (-1)^m (2n-3-2m)!! \right. \\ &\quad \times \sum_{C_n^{2m} (2m-1)!!} (\delta_{t_1 t_2} \delta_{t_3 t_4} \dots \delta_{t_{2m-1} t_{2m}} \\ &\quad \left. \times g_{t_{2m+1}} g_{t_{2m+2}} \dots g_{t_n} \right\}, \end{aligned} \quad (\text{A7})$$

where t_1, t_2, \dots, t_{2m} are a group of indices selected from a_n in a permutation manner, and t_{2m+1}, \dots, t_n are the other group of a_n after such a selection. The summation $\sum_{C_n^{2m} (2m-1)!!}$ means taking sum over all combinations.

By defining

$$\mathbf{1} = \{e_i\} \quad (\text{A8})$$

and

$$\mathbf{R}^{(n)} = \{R_{,a_1 a_2 \dots a_n}\} \quad (\text{A9})$$

we can write Eq. (A7) as

$$\begin{aligned} \mathbf{R}^{(n)} &= \left(\frac{-1}{R} \right)^{n-1} \sum_{m=0}^{\lfloor n/2 \rfloor} \left\{ (-1)^m (2n-3-2m)!! \right. \\ &\quad \left. \times \sum_{C_n^{2m} C_{2m}^2} [(\mathbf{\Pi} \otimes^{n-2m} \mathbf{g}) (\mathbf{\Pi} \otimes^{2m} \mathbf{1})] \right\}. \end{aligned} \quad (\text{A10})$$

In this equation, m is the number of δ 's and is from 0 to $|n/2|$ which indicates the largest integer not larger than $n/2$. The symbol $\Pi \otimes^n$ indicates that there are a number of n items of \mathbf{g} or $\mathbf{1}$ with the operation \otimes . The second summation $\sum C_n^{2m} C_{2m}^2$ means doing summing in a permutation and combination manner, with the number of items $\mathbf{1}$ as $2m$ and the number of items \mathbf{g} as $n-2m$. For example, with $m=1$ and $n=4$, we have

$$\begin{aligned}
 & C_n^{2m} (2m-1)!! \\
 & \sum [(\Pi \otimes^{n-2m} \mathbf{g})(\Pi \otimes^{2m} \mathbf{1})] \\
 & = \sum_{C_4^2} [(\Pi \otimes^2 \mathbf{g})(\Pi \otimes^2 \mathbf{1})] = \mathbf{1} \otimes \mathbf{1} \otimes \mathbf{g} \otimes \mathbf{g} + \mathbf{1} \otimes \mathbf{g} \otimes \mathbf{1} \otimes \mathbf{g} + \mathbf{1} \\
 & \quad \otimes \mathbf{g} \otimes \mathbf{g} \otimes \mathbf{1} + \mathbf{g} \otimes \mathbf{1} \otimes \mathbf{1} \otimes \mathbf{g} + \mathbf{g} \otimes \mathbf{1} \otimes \mathbf{g} \otimes \mathbf{1} + \mathbf{g} \otimes \mathbf{g} \otimes \mathbf{1} \otimes \mathbf{1}.
 \end{aligned} \tag{A11}$$

¹N. Ghoniem and R. Amodeo, *Solid State Phenom.* **3&4**, 377 (1988).

²N. Ghoniem and L. Sun, *Phys. Rev. B* **60**, 128 (1999).

³N. Ghoniem, S. Tong, and L. Sun, *Phys. Rev. B* **61**, 913 (2000).

⁴B. Devincere and L.P. Kubin, *Philos. Trans. R. Soc. London* **355**, 2003 (1997).

⁵B. Devincere and L. Kubin, *Mater. Sci. Eng., A* **234-236**, 8 (1997).

⁶H.M. Zbib, M. Rhee, and J.P. Hirth, *Int. J. Mech. Sci.* **40**, 113 (1998).

⁷K. Schwarz, *J. Appl. Phys.* **85**, 108 (1999).

⁸N.M. Ghoniem, H. Huang, E. Busso, and N. Kioussis, *Philos. Mag.* **83**, 3475 (2003).

⁹N.M. Ghoniem and K. Cho, *J. Comp. Meth. Engr. Science* **3**, 147

(2002).

¹⁰R. Lesar and J.M. Rickman, *Phys. Rev. B* **65**, 144110 (2002).

¹¹V. Rokhlin, H. Cheng, and L. Greengard, *J. Comput. Phys.* **155**, 468 (1999).

¹²E. Kröner, in *Physics of Defects*, edited by R. B. *et al.*, (North-Holland, Amsterdam, 1981).

¹³N. Ghoniem, J. Huang, and Z. Wang, *Philos. Mag. Lett.* **82**, 55 (2002).

¹⁴J. Nye, *Acta Metall.* **1**, 153 (1953).

¹⁵A. Arsenlis and D. Parks, *Acta Mater.* **47**, 1597 (1999).

¹⁶L. Greengard and V. Rokhlin, *J. Comput. Phys.* **73**, 325 (1987).

¹⁷D.A. Hughes, S.M. Khan, A. Godfrey, and H.M. Zbib, *Mater. Sci. Eng., A* **309-310**, 230 (2001).